Comparative Study of Soluble Naphthalene Diimide Derivatives Bearing Long Alkyl Chains as n-type Organic Thin-Film Transistor Materials

Musubu Ichikawa[1,2,*], Yoichiro Yokota[1], Hyeon-Gu Jeon[1†], Gilles de Romeo Banoukepa[1,3], Naoki Hirata[4], Naomi Oguma[4]

[1]*Interdisciplinary Graduate School of Science and Technology, Shinshu University, 3-15-1 Tokida, Ueda City, Nagano 386-8567, Japan*

[2]*Presto, Japan Science and Technology Agency (JST), 4-8-1 Honcho, Kawaguchi, Saitama 332-0012, Japan*

[3]*Japan Society for the Promotion of Science, 8 ichibancho, Chiyoda, Tokyo 102-8472, Japan*

[4]*Dainichiseika Color & Chemicals Mfg. Co., Ltd. 1-9-4, Horinouchi, Adachi-ku, Tokyo, 123-8588, Japan*

Abstract: In this study, several naphthalene tetracarboxylic acid diimide (NTCDI)

derivatives substituted at the N and N' positions with long normal alkyl chains of different lengths were evaluated as soluble n-type organic thin-film transistor (TFT) materials. NTCDI derivatives with diundecyl (NTCDI-C11), didodecyl (NTCDI-C12), and ditridecyl (NTCDI-C13) exhibited acceptable solubility in chloroform, and their TFTs showed typical n-type TFT performance with relatively high field effect electron mobility (~0.2 cm^2/Vs) after annealing at a workable temperature of 150 °C. Although NTCDI with dioctyl (NTCDI-C8) showed good solubility in chloroform, the TFT performance of this material was highly inferior to that of NTCDI-C11, NTCDI-C12, or NTCDI-C13. We could not anneal NTCDI-C8 thin films at workable temperatures in vacuo because of sublimation of the material from the substrates. In contrast, NTCDI with dipentadecyl (NTCDI-C15) and dioctadecyl (NTCDI-C18) exhibited both poor solubility for chloroform and poor TFT performance. In short, these compounds are not suitable as soluble n-type organic TFT materials.

*Corresponding author at: Interdisciplinary Graduate School of Science and Technology, Shinshu University, 3-15-1 Tokida, Ueda City, Nagano 386-8567, Japan

Tel: +81-268-21-5498; Fax: +81-268-21-5417

Email address: musubu@shinshu-u.ac.jp

†Present address: *Department of Materials Science and Biotechnology, Graduate School of Science and Engineering, Ehime University, Matsuyama 790-8577, Japan*

1. Introduction

Recently, the commercialization of organic thin-film transistors (TFTs) has attracted wide attention because of their potential in next-generation electronic devices such as flexible displays and low-cost radio-frequency identification tags.[1] Although significant progress has been made in research into organic TFTs during the last few decades[2-5] to facilitate viable commercialization, there is still a need for further improvement in not only device performance but also other factors such as operating stability and device reproducibility.[6, 7] One particular target is the development of soluble n-type materials with high device performance.[8-10] This is highly desirable for the formation of high-performance complementary circuits composed of p- and n-channel TFTs having similar performance[11] and for the realization of low manufacturing costs in real terms using solution processes, which is one of the greatest potential benefits of organic semiconductors.[12]

Perylene tetracarboxylic acid diimides (PTCDIs) are among the most promising n-channel candidates for organic TFTs because of their high electron affinity and large π-orbital overlap in the solid state.[9, 10, 13-19] Many substituents have been introduced in PTCDIs to, for example, improve electron mobility, enlarge electron affinity for operation stability in air, and improve solubility in common solvents. Solubility is one of the most important properties of organic semiconductors because solution processes are crucial to low-cost and large-area manufacturing procedures. Although alkyl groups have no function electronically, they are commonly utilized as substituents in order to improve solubility. However, simple PTCDIs with normal alkyl

chains at the N and N' positions barely achieve the solubility in widely used solvents, such as chloroform, required for the preparation of organic semiconductor thin films. This is because the PTCDI core is too large to modify its solubility through the substitution of normal alkyl chains alone. However, naphthalene tetracarboxylic acid diimide (NTCDI) is an analog of PTCDI that has a reduced π-electron system compared with that of PTCDI, and has received increasing attention as a building block for soluble n-type organic semiconductors.[8, 20-25] However, we believe that there are currently no reports that compare NTCDI derivatives bearing normal alkyl chains with varying lengths at the N and N' positions. The small π-electron core ensures solubility in chloroform even if normal alkyl groups are used as the substituents, allowing investigation of the influence of alkyl chain length. In this study, we compare the TFT performance of several NTCDI derivatives (NTCDI-Cn; n = 8, 11, 12, 13, 15, and 18, see Fig. 1) bearing normal alkyl chains with different lengths at the N and N' positions.

Molecules coupled with a rigid π-electron core and alkyl chains frequently exhibit thermotropic liquid crystalline mesophases. Furthermore, molecules move easier in liquid crystal phases than in solid phases because of higher fluidity. As a result, well-aligned molecular orientations and packing, which are critical for charge-carrier transport [26-28] in organic semiconductor thin films, can be attained after thermal annealing of the thin-films. In this study, we thermally treated NTCDI-Cn thin films prepared by a solution process. Although annealing based on solvent vapor (solvent vapor annealing) is widely used, especially in solution-processed organic semiconductor thin films [29-31], we opted for simple thermal annealing in this study.

5

2. Experimental

NTCDI-Cn derivatives were synthesized from naphthalene-1,4,5,8-teracalboxylic acid dianhydride (NTCDA) and the corresponding alkylamine according to a method adapted from the literature[22]. Both reactants (NTCDA:amine = 1:2.5 in mole) were mixed in dimethylformamide (DMF) at an NTCDA concentration of approximately 5wt% and refluxed for 12 h. The precipitates obtained, which were orange because an orange over-reacted product (tetraamide) was included as an impurity, were washed with ethanol several times. After drying, the organic residues were purified using a Japan Analytical Industries (JAI) recycling preparative high-performance liquid chromatography (HPLC) instrument (LC-9104) with a gel permeation chromatography column (JAI, JAIGEL 1H-40). Chloroform was used as an eluent if the obtained NTCDI derivative had sufficient solubility in chloroform (NTCDI-C15 and -C18 had insufficient solubility to perform the column purification). Thermal analyses of the materials were performed on a differential scanning calorimeter (Seiko Instruments DSC-6200) at a heating rate of 10 °C/min under N_2 gas.

NTCDI-Cn thin films were prepared by spin coating on silicon wafers with a 200-nm-thick SiO_2 layer as the gate dielectric and patterned indium tin oxide (ITO) as the source and drain electrodes on the SiO_2 layer, as shown in Fig. 1. The width (W) and length (L) of the channels were 100 μm and 1.5 mm, respectively, and the specific capacitance (C_i) of the gate dielectric was 18 nF/cm^2. The NTCDI-Cn active layer covers almost all the surface of the gate dielectric, whereas the large W/L ratio of 15

6

assures an ignorable influence due to the current flow of the outer sides of the electrodes. The preparation of the ITO-patterned Si wafers is described elsewhere.[32] The prepared Si wafers were washed before use by ultrasonication in 2-propanol, and no surface treatment was done on the surface as we intended to prepare uniform NTCDI-Cn thin films. The surface treatment with silane coupling reagents such as octadecylsilyl trichloride was difficult because of the high solvent repellency of the treated surfaces. Prior to the thin film preparation, NTCDI-Cn was dissolved in chloroform at a concentration of 0.5 wt% at room temperature for NTCDI-C8, -C11, and -C12; at a concentration of 0.5 wt% at 50 °C for NTCDI-C13; or at a concentration of 0.25 wt% at 50 °C for NTCDI-C15 and -C18. The coating conditions were 1500 rpm for 60 s. The thickness of the thin films was in the order of several tens of nanometers, depending on the concentration of NTCDI. The as-spun thin films were dried in a vacuum oven at room temperature. After drying, the thin films were annealed in the oven at particular temperatures from 100 to 170 °C for 1 h. An Agilent semiconductor parameter analyzer (B1500A) recorded the performance of the TFTs generated in dark and under vacuum. We also prepared other thin films for measuring surface morphologies. A Bruker scanning probe microscope (Dimension ICON PTX) and a Rigaku rotaflex X-ray diffractometer with Cu-Kα radiation (154 pm) revealed surface morphologies and X-ray diffraction (XRD) patterns of NTCDI-Cn thin films, which were simultaneously prepared on other Si wafers with the SiO_2 layer in the absence of ITO for each TFT preparation.

3. Results and Discussion

3.1 NTCDI-C13

Fig. 2a shows drain current (I_D)–drain voltage (V_D) characteristics of the NTCDI-C13 TFT annealed at 150 °C. The TFT exhibited typical n-type field-effect transistor behavior: almost linear increases in drain current at the low drain voltage region and saturation of the current at a higher voltage region as shown in the figure. Fig. 2b shows the I_D–gate voltage (V_G) and $(I_D)^{1/2}$–V_G curves at V_D = 100 V. The TFT exhibited hysteresis, which implies that there are charge-carrier traps at the interface, which might result from the silanol groups on the bear SiO_2 surface.[33] Therefore, we analyzed the forward half (from 0 to 100 V) of the I_D–V_G curves in this study. The field effect mobility mobility (μ_{FE}) was obtained from the saturated drain current ($I_{D,sat}$) by using the following equation:

$$I_{D,sat} = \frac{W}{2L} C_i \mu_{FE} (V_G - V_T)^2 , \tag{1}$$

where V_T is the threshold voltage. The mobility and V_T were 0.21 cm^2/Vs and 25 V, respectively. The field effect mobility is comparable with that of amorphous silicon TFTs ($\mu \sim$ 0.5 cm^2/Vs). This relatively high electron μ_{FE} of NTCDI-C13, which was obtained from a solution process, indicates that NTCDI-C13 has good potential as a TFT material. In addition, the mobility is also comparable with that of perylenediimide (PTCDI)-based solution-processable organic TFT materials reported recently by our group (~0.5 cm^2/Vs),[10] while PTCDI has a larger π-electronic skeleton than NTCDI.

Fig. 3 shows the annealing-temperature (T_A) dependence of μ_{FE} and V_T of the NTCDI-C13 TFTs. The TFT without annealing showed low μ_{FE} and high V_T. In contrast, the annealed TFTs showed much higher μ_{FE} and lower V_T, while higher T_A led to higher μ_{FE} and lower V_T up to a T_A of 150 °C. However, further increases in T_A above 150 °C induced no transistor behavior. The melting point of NTCDI-C13 is 161 °C, and the molten NTCDI-C13 thin film on the surface is dewetted as shown in Fig. S1, possibly because of the large difference in the surface free energies of NTCDI-C13 and SiO_2.

Fig. 4 shows surface morphologies of the NTCDI-C13 thin films annealed at different temperatures. While needle-like grains appeared in the as-spun NTCDI-C13 thin film, all the annealed thin films showed a completely different morphology. There were round plate-like grains in whole surfaces, and large flat domains that were present in layers spread under the plate-like grains. Larger grains are known to be preferable from the perspective of higher charge carrier mobility. Thus, the large flat domains probably cause relatively high electron mobility in the annealed thin films, and the change in morphologies results in increasing electron μ_{FE}. In addition, the decrease in V_T with increasing T_A might also be caused by the morphological change and the growth of the grains.

In addition, the large flat domains in the layers exhibited 2.8-nm-high steps all over the surfaces, particularly on the surface of the thin film (T_A = 150 °C). The step height of 2.8 nm corresponded to the d spacing (2.85 nm) of the largest signal at 2θ = 3.1° in the XRD pattern of the thin films (T_A = 150 °C), as shown in Fig. 5. Therefore, the large flat domains that appear after annealing and probably cause relatively high

electron μ_{FE} represent a highly ordered molecular layer-by-layer phase. A quantum chemical calculation suggested a molecular length of NTCDI-C13 (the distance between the hydrogen atoms at both ends) of 4.072 nm, as shown in Fig. S2. This means that NTCDI-C13 molecules in the thin films are oriented approximately 47° to the normal of the substrate plane. Although the X-ray crystallographic analysis of this material has not yet been performed, from an analogical consideration with the crystal structure of N,N'-ditridecyl PTCDI (PTCDI-C13)[34], molecular alignments in this flat domain can be depicted as shown in the inset of Fig. 5. A small tilt angle (15°) of the NTCDI core can be reasonably assumed, which is expected to be preferable for charge transportation between molecules.

Fig. 6 shows the DSC curve of NTCDI-C13 powder. Although the strongest endothermic peak at 162 °C could be assigned as a transition to its isotropic liquid (IL), the other endothermic peaks at 109 and 144 °C are not clear at present because of the limitations of our experimental instruments. However, visual observation during the measurement of IL temperature suggested that the transitions at 109 and 144 °C were from one crystalline phase to another (K–K) and from the second crystalline phase to a liquid crystal phase (K–LC), respectively. There are several reports of organic TFTs based on materials with an LC phase that display performance enhancements after annealing above the transition temperature to their LC phase, because of dramatic changes in film morphology.[18, 35] We believe that the μ_{FE} enhancements and morphological changes after annealing partly result from high molecular mobility in the LC phase, although another factor might also be responsible because the enhancement

and morphological changes were observed even at a T_A of 100 °C. The small molecular size of the NTCDI core, whose molecular weight is 266 g/mol, compared with that of PTCDI might influence the high molecular mobility, which is crucial for dramatic morphological changes.

3.2 NTCDI with Other Alkyl Lengths: NTCDI-C11 and C12

Fig. 7 shows the T_A dependence of electron μ_{FE} and V_T of NTCDI-C11 and C12 TFTs. The TFTs also showed enhanced mobilities and lowered V_T after annealing. The same tendencies appeared in NTCDI-C13 TFTs, as shown in Fig. 3. As shown in Fig. 8, morphologies of the thin films of both NTCDI-C11 and -C12 dramatically changed after annealing. Large flat domains, which also appeared in the NTCDI-C13 thin films after annealing, appeared. Steps with a height of approximately 2.7–2.8 nm were observed at the edges of the large flat domains, as in the case of NTCDI-C13. The height almost corresponded to XRD d spacings of 2.66 nm for NTCDI-C11 and 2.71 nm for NTCDI-C12. Note that the d spacings of the three materials subsequently decreased with the length of alkyl chains, indicating that the molecular alignments in the large domains for the three materials would be almost identical.

Table 1 summarizes phase transition temperatures of NTCDI-C11 and -C12. As shown in the table, the last transition temperatures of NTCDI-C11, -C12, and -C13 to its IL inversely depended on the number of carbon atoms in the alkyl chains. This suggests that the phase before the transition might be LC, as already described. Visual observations of NTCDI-C11 and C12 powders in glass capillaries at a temperature

slightly below each transition temperature to IL identified an opaque liquid, a typical characteristic of an LC, which supported the hypothesis that the transition temperatures of NTCDI-C11 and -C12 were from LC to IL. In short, the transition temperatures at 148 °C for -C11 and 147 °C for -C12 were from crystal to LC. Note that NTCD-C11 exhibited another transition because of a crystal structure change (K–K) at 102 °C. As shown in Table 1, only NTCDIs bearing alkyl chains with an odd number of carbons showed this type of transition.

As shown in Fig. 8, growths of large flat domains of NTCDI-C11 and -C12 began below the corresponding K–LC transitions, and μ_{FE} improvements could be observed by T_A = 100 °C, as described previously. NTCDI-C13 and -C11 have K–K transitions at approximately 100–110 °C, but the transitions could not cause the morphological change and μ_{FE} enhancement, which occurred at T_A = 100 °C. This is because NTCDI-C12 has no such K–K transition. Therefore, compared with other organic semiconductors, the relatively small molecular size and weight of the NTCDI core probably allows the molecules to move freely even in their crystalline thin-film state at lower annealing temperatures of approximately 100 °C. In addition, several clear and deep boundaries appeared in the NTCDI-C11 thin film annealed at 150 °C, as shown in panel (c) of Fig. 8. The boundaries probably affect the electron transport in the film, but we currently cannot explain why they appeared and how they influence the transportation process. This is because the clear and deep boundaries were observed only in NTCDI-C11 thin films.

3.3 NTCDI with Shorter and Longer Alkyl Lengths: NTCDI-C8, -C15, and -C18

Fig. 9 shows the electron mobilities of NTCDI-Cn TFTs after annealing at various temperatures. As presented in the figure, NTCDI-C8 TFTs clearly exhibited lower μ_{FE} than NTCDI-C11-13 TFTs. Note that NTCDI-C8 TFTs at T_A = 150 °C showed no TFT performance because of sublimation of the thin films during the annealing process. In contrast, NTCDI derivatives with longer alkyl chains (NTCDI-C15 and -C18) exhibited very poor TFT performances. We believe that the most important reason for these very poor performances might be the low solubility of the materials in solvents, which limited the preparation of thin films with sufficient quality. Thus, it is concluded that the optimal alkyl length probably ranges from 11 to 13.

3.4 Comparison of NTCDI-C11 to -C13

Among the optimal range of alkyl chain lengths, it was interesting to compare the chain-length dependence of electron μ_{FE} at each T_A. As shown in Fig. 9, the increasing length led to decreased μ_{FE} at T_A = 100 °C. In contrast, no length dependence was observed at T_A = 125 °C, and an almost converse tendency was observed at T_A = 150 °C compared with that at T_A = 100 °C. This behavior suggests that a longer alkyl length prevents any increase in molecular mobility at a low T_A of approximately 100 °C owing to its larger molecular weight and/or interactions between the alkyl chains. The electron μ_{FE} improvement of NTCDI-C13 at T_A = 150 °C against that at T_A = 100 °C

was larger than that of NTCDI-C11 and -C12, and the electron μ_{FE} of NTCDI-C13 was the best overall. In accordance with our former report, the higher molecular mobility due to the shorter alkyl chains leads to excessive thin-film reconstructions, which results in defective thin films having deficient parts because molecules have migrated to other parts.[18] From this perspective, NTCDI-C13 must be the optimal n-type material, with its relatively high electron μ_{FE} and wet-process capability.

4. Summary

Several NTCDI derivatives substituted at the N and N' positions with long normal alkyl chains of varying lengths were evaluated as active materials for n-type organic TFTs. NTCDI with diundecyl (NTCDI-C11), didodecyl (NTCDI-C12), and ditridecyl chains (NTCDI-C13) exhibited acceptable solubility in chloroform, and their TFTs showed typical n-type TFT performance with relatively high electron μ_{FE} (~0.2 cm^2/Vs) after annealing at the workable temperature of 150 °C. Although NTCDI with dioctyl (NTCDI-C8) showed good solubility in chloroform, its performance was greatly inferior to that of NTCDI-C11, NTCDI-C12, or NTCDI-C13 from the perspective of TFT performance. We could not anneal NTCDI-C8 thin films at a workable temperature in vacuo because of sublimation of the material from the substrates. In contrast, NTCDI with dipentadecyl (NTCDI-C15) and dioctadecyl chains (NTCDI-C18) exhibited both poor solubility for chloroform and poor TFT performance. In short, these compounds are not suitable as soluble n-type organic TFT materials. However, if thin films with these materials can be successfully obtained, there is a possibility of achieving much

14

better TFT performances after annealing.

References

[1]   G. Gelinck, P. Heremans, K. Nomoto, T. D. Anthopoulos, Adv. Mater. **22** (2010) 3778.

[2]   C. D. Dimitrakopoulos, P. R. L. Malenfant, Adv. Mater. **14** (2002) 99.

[3]   S. Ando, R. Murakami, J.-i. Nishida, H. Tada, Y. Inoue, S. Tokito, Y. Yamashita, J. Am. Chem. Soc. **127** (2005) 14996.

[4]   K. Takimiya, H. Ebata, K. Sakamoto, T. Izawa, T. Otsubo, Y. Kunugi, J. Am. Chem. Soc. **128** (2006) 12604.

[5]   J. Zaumseil, H. Sirringhaus, Chem Rev **107** (2007) 1296.

[6]   R. A. Street, Adv. Mater. **21** (2009) 2007.

[7]   Y. Wen, Y. Liu, C.-a. Di, Y. Wang, X. Sun, Y. Guo, J. Zheng, W. Wu, S. Ye, G. Yu, Adv. Mater. **21** (2009) 1631.

[8]   W.-Y. Lee, J. H. Oh, S.-L. Suraru, W.-C. Chen, F. Würthner, Z. Bao, Adv. Funct. Mater. **21** (2011) 4173.

[9]   H.-W. Ting, S.-Y. Chen, T.-C. Huang, J.-H. Wei, T.-R. Yew, ChemPhysChem **12** (2011) 871.

[10] H.-G. Jeon, Y. Yokota, J. Hattori, N. Oguma, N. Hirata, T. Suzuki, M. Ichikawa*,

Appl. Phys. Express **5** (2012) 041602.

[11] J. E. Anthony, A. Facchetti, M. Heeney, S. R. Marder, X. Zhan, Adv. Mater. **22** (2010) 3876.

[12] H. Klauk, Organic Electronics: Materials, Manufacturing and Applications,. Wiley-VCH: Weinheim, 2006.

[13] G. Horowitz, F. Kouki, P. Spearman, D. Fichou, C. Nogues, X. Pan, F. Garnier, Adv. Mater. **8** (1996) 242.

[14] P. R. L. Malenfant, C. D. Dimitrakopoulos, J. D. Gelorme, L. L. Kosbar, T. O. Graham, Appl. Phys. Lett. **80** (2002) 2517.

[15] B. A. Jones, M. J. Ahrens, M.-H. Yoon, A. Facchetti, T. J. Marks, M. R. Wasielewski, Angew. Chem. Int. Ed. **43** (2004) 6363.

[16] S. Tatemichi, M. Ichikawa, T. Koyama, Y. Taniguchi, Appl. Phys. Lett. **89** (2006) 112108.

[17] M.-M. Ling, P. Erk, M. Gomez, M. Koenemann, J. Locklin, Z. Bao, Adv. Mater. **19** (2007) 1123.

[18] H.-G. Jeon, J. Hattori, S. Kato, N. Oguma, N. Hirata, Y. Taniguchi, M. Ichikawa, J. Appl. Phys. **108** (2010) 124512.

[19] X. Zhan, A. Facchetti, S. Barlow, T. J. Marks, M. A. Ratner, M. R. Wasielewski, S. R. Marder, Adv. Mater. **23** (2011) 268.

[20] H. E. Katz, A. J. Lovinger, J. Johnson, C. Kloc, T. Siegrist, W. Li, Y.-Y. Lin, A. Dodabalapur, Nature **404** (2000) 478.

[21] B. A. Jones, A. Facchetti, T. J. Marks, M. R. Wasielewski, Chem. Mater. **19** (2007) 2703.

[22] D. Shukla, S. F. Nelson, D. C. Freeman, M. Rajeswaran, W. G. Ahearn, D. M. Meyer, J. T. Carey, Chem. Mater. **20** (2008) 7486.

[23] Y.-L. Lee, H.-L. Hsu, S.-Y. Chen, T.-R. Yew, J. Phys. Chem. C **112** (2008) 1694.

[24] J. H. Oh, S. L. Suraru, W.-Y. Lee, M. Könemann, H. W. Höffken, C. Röger, R. Schmidt, Y. Chung, W.-C. Chen, F. Würthner, Z. Bao, Adv. Funct. Mater. **20** (2010) 2148.

[25] I. Tszydel, M. Kucinska, T. Marszalek, R. Rybakiewicz, A. Nosal, J. Jung, M. Gazicki-Lipman, C. Pitsalidis, C. Gravalidis, S. Logothetidis, M. Zagorska, J. Ulanski, Adv. Funct. Mater. **22** (2012) 3840.

[26] F. Garnier, G. Horowitz, D. Fichou, A. Yassar, Synth. Met. **81** (1996) 163.

[27] Y. Y. Lin, D. J. Gundlach, S. F. Nelson, T. N. Jackson, IEEE Electr Device L **18** (1997) 606.

[28] J. Takeya, M. Yamagishi, Y. Tominari, R. Hirahara, Y. Nakazawa, T. Nishikawa, T. Kawase, T. Shimoda, S. Ogawa, Appl. Phys. Lett. **90** (2007) 102120.

[29] K. C. Dickey, J. E. Anthony, Y. L. Loo, Adv. Mater. **18** (2006) 1721.

[30] Y. Fu, C. Lin, F.-Y. Tsai, Org. Electron. **10** (2009) 883.

[31] C. Liu, T. Minari, Y. Li, A. Kumatani, M. V. Lee, S. H. Athena Pan, K. Takimiya, K. Tsukagoshi, J. Mater. Chem. **22** (2012) 8462.

[32] M. Ichikawa, K. Yamamura, H.-G. Jeon, M. Nakajima, Y. Taniguchi, J. Appl. Phys. **109** (2011) 054504.

[33] L. L. Chua, J. Zaumseil, J. F. Chang, E. C. W. Ou, P. K. H. Ho, H. Sirringhaus, R. H. Friend, Nature **434** (2005) 194.

[34] M. Ichikawa, L. You, S. Tatemichi, T. Koyama, Y. Taniguchi, Jpn J. Appl. Phys.

45 (2006) L1171.

[35] T. Umeda, S. Tokito, D. Kumaki, J. Appl. Phys. **101** (2007) 054517.

Figure Captions

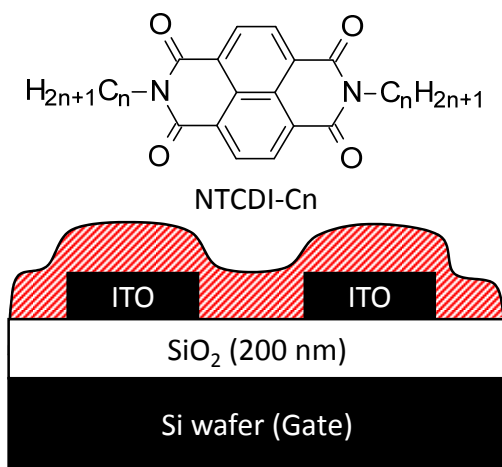Table 1. Phase transition behavior of NTCDI-Cn derivatives

Figure 1. Chemical structure of NTCDI-Cn and schematic cross section of TFTs prepared in this study.
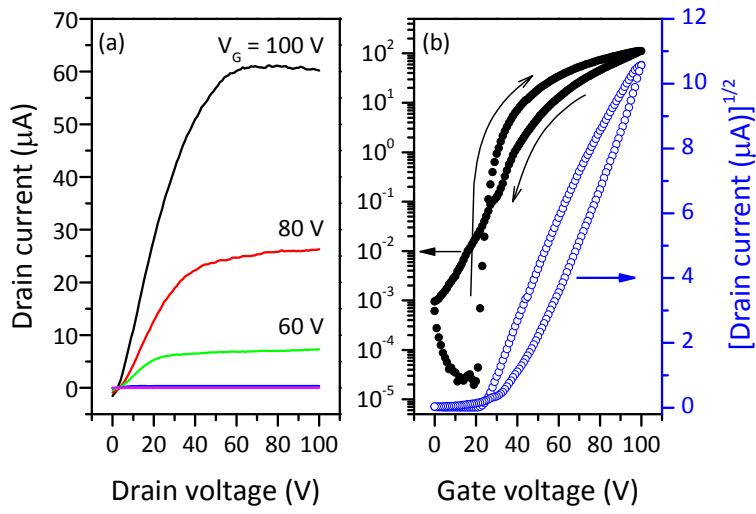
Figure 2. I_D–V_D (a) and I_D–V_G (b) characteristics of NTCDI-C13 TFT annealed at 150 °C. The I_D–V_G characteristic was measured at $V_D = 100$ V
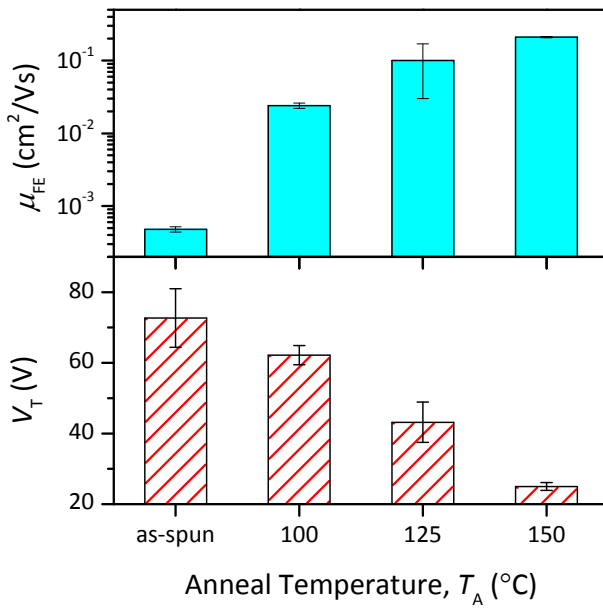
Figure 3. Anneal-temperature dependence of field effect mobility (μ_{FE}) and threshold voltage (V_T) of NTCDI-C13 TFT.
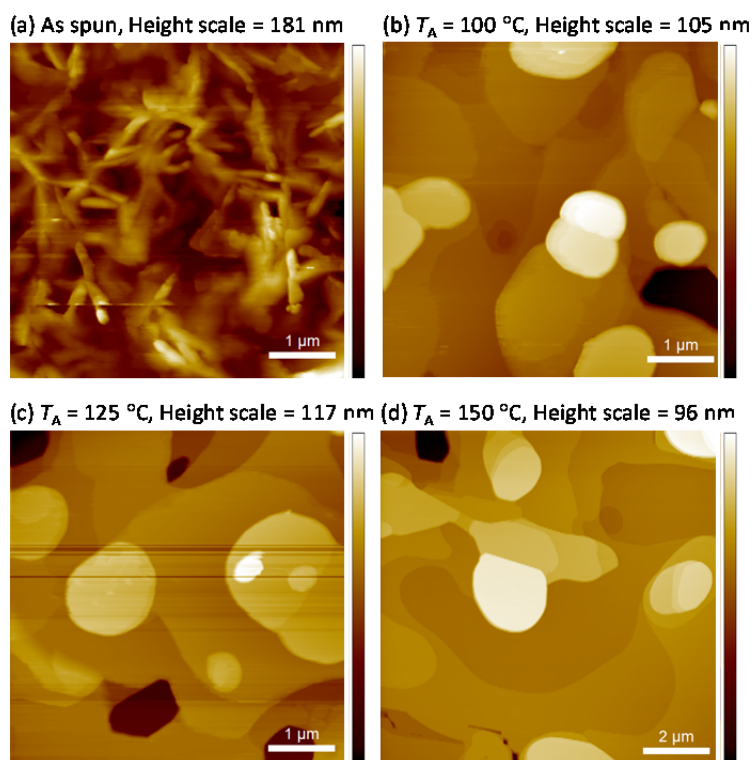
Figure 4. Surface morphologies of NTCDI-C13 thin films after annealing at several temperatures. A film as-spun (no annealing) is also presented.

Figure 5. XRD patterns of NTCDI-C13 thin films with and without annealing.

Figure 6. DSC curve of NTCDI-C13 powder. The numbers in the panel represent transition temperature and phase.

18

Figure 7. T_A dependence of μ_{FE} and V_T of NTCDI-C11 and -C12 TFTs after annealing. The legend of the lower panel is the same as that of the upper one.

Figure 8. Surface morphologies of NTCDI-C11 (a–c) and -C12 (d–f) thin films after annealing and with no annealing (as-spun).

Figure 9. Alkyl-chain-length dependence of the field effect mobility of NTCDI-Cn TFTs after annealing at various temperatures.

Table 1. Phase transition behavior of NTCDI-Cn derivatives

NTCDI-Cn	Transition Temperature (°C)		
	K–K	K–LC	LC–IL
C8		171.1	185.1
C11	104.5	148.2	169.8
C12		146.9	165.7
C13	109.2	143.6	162.3
C15	114.2	139.6	156.2
C18		138.4	148.9

Figure 1. Chemical structure of NTCDI-Cn and schematic cross section of TFTs prepared in this study.

Figure 2. I_D–V_D (a) and I_D–V_G (b) characteristics of NTCDI-C13 TFT annealed at 150 °C. The I_D–V_G characteristic was measured at $V_D = 100$ V

Figure 3. Anneal-temperature dependence of field effect mobility (μ_{FE}) and threshold voltage (V_T) of NTCDI-C13 TFT.

Figure 4. Surface morphologies of NTCDI-C13 thin films after annealing at several temperatures. A film as-spun (no annealing) is also presented.
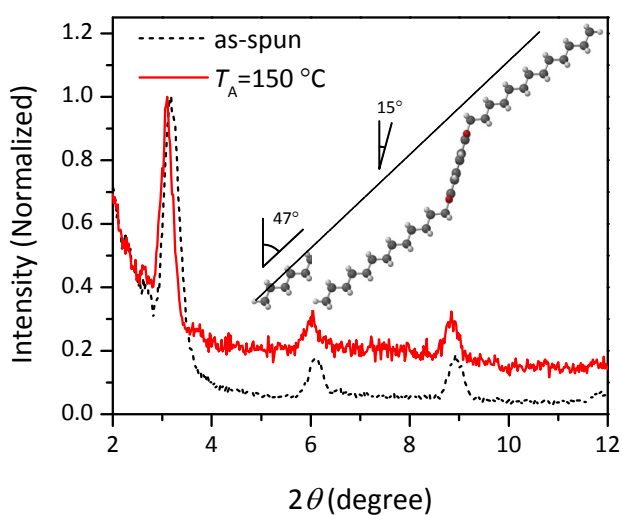

Figure 5. XRD patterns of NTCDI-C13 thin films with and without annealing.

Figure 6. DSC curve of NTCDI-C13 powder. The numbers in the panel represent transition temperature and phase.
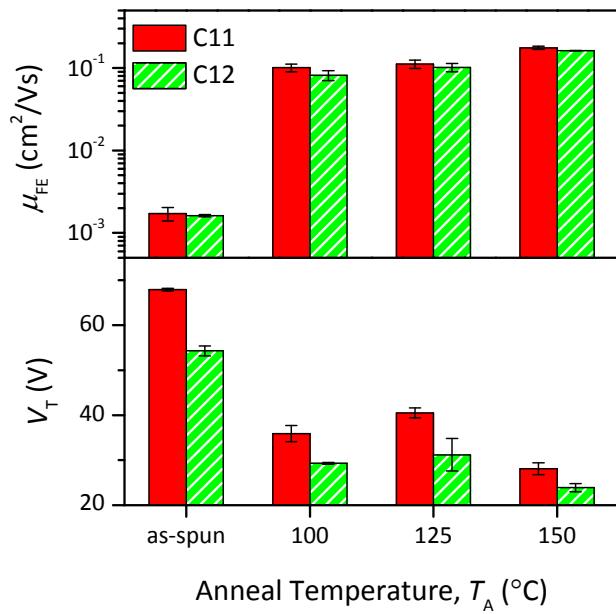

Figure 7. T_A dependence of μ_{FE} and V_T of NTCDI-C11 and -C12 TFTs after annealing. The legend of the lower panel is the same as that of the upper one.
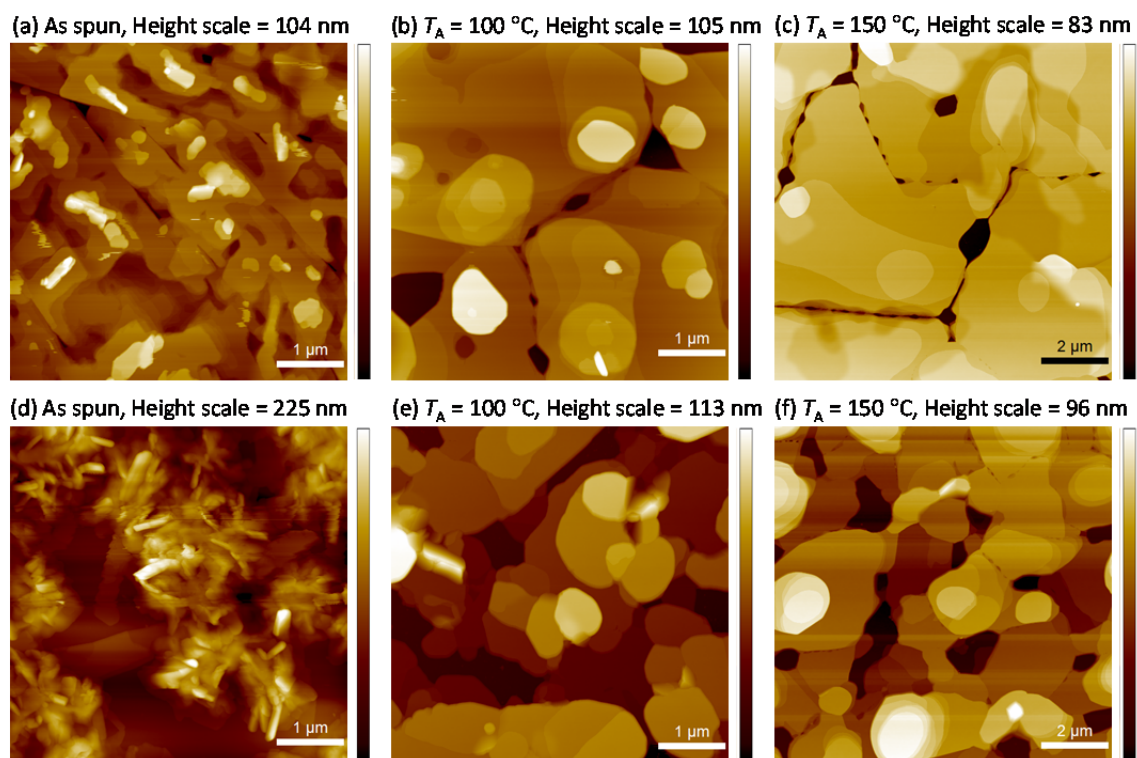
Figure 8. Surface morphologies of NTCDI-C11 (a–c) and -C12 (d–f) thin films after annealing and with no annealing (as-spun).
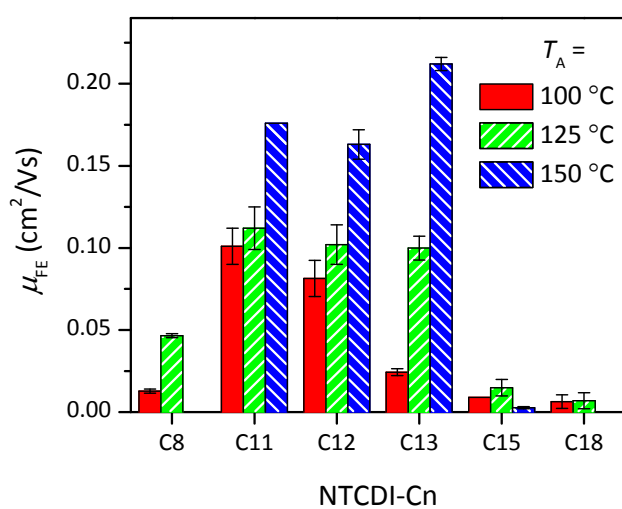

Figure 9. Alkyl-chain-length dependence of the field effect mobility of NTCDI-Cn TFTs

after annealing at various temperatures.